Design and Optimization of Fluid Supply Flow Paths for a Balanced Twin-Lip Vane Pump

Jinglun Qu[a,*], Andrea Vacca[a,b], Sri Krishna Uppaluri[c]

[a] *School of Mechanical Engineering, Purdue University, West Lafayette, 47907, IN, USA*

[b] *School of Agricultural and Biological Engineering, Purdue University, West Lafayette, 47907, IN, USA*

[c] *Veljan Denison Limited, A18 and 19, APIE, Balanagar, Hyderabad, 500037, Telangana, India*

[*] *Corresponding author: qu134@purdue.edu*

Abstract

This paper presents a methodology for designing and optimizing the fluid supply flow path of a balanced twin-lip vane pump, supported by experimental validation. Cavitation in the suction port, caused by insufficient fluid supply to the displacement chamber, is a leading cause of pump failure due to the severe damage it inflicts on critical components. This paper includes the further development of a previously established numerical model to consider the complex supply path of the casing. The methodology utilizes preliminary Computational Fluid Dynamics (CFD) simulations to characterize the hydraulic resistance of the upstream orifices and chambers. The baseline model was validated against existing experimental results to confirm its fidelity. The updated extended model successfully captures the localized cavitation effects occurring within the casing, leading to proposed geometry updates. By characterizing the new design using CFD, the model demonstrates significantly improved supply flow capabilities. Further updates of the cam-ring orifice were conducted, and simulation results predict the substantially improved performance of the pump at maximum operating speeds, which is experimentally validated in this study.

Keywords: Vane pump, Fluid supply flow paths, Cavitation, Lumped parameter model, Computational Fluid Dynamics.

Nomenclature

Symbols

A	Cross-sectional area [m^2]
C_d	Discharge coefficient [-]
c_e	Coefficient of restitution [-]
E	Young's modulus [Pa]
η	Efficiency [-]
K	Fluid bulk modulus [Pa]
$\dot{m}$	Mass flow rate [kg/s]
p	Pressure [Pa]
Δp	Differential pressure drop [Pa]
Q	Flow rate [L/min]
Re_{crit}	Critical Reynolds number [-]
T	Temperature [°C]
t	Time [s]
V	Volume [m^3]
α_{air}	Dissolved air volume fraction [-]
α_{gas}	Gas volume fraction [-]
ν	Kinematic viscosity [m^2/s]
ρ	Fluid density [kg/m^3]
Ω	Normalized operating speed [RPM]

Subscripts

atm	Atmospheric conditions
CFD	Computed via Computational Fluid Dynamics
i, j	Control volume or chamber indices
in	Inlet
max	Maximum
nom	Nominal
out	Outlet
vol	Volumetric

Abbreviations

CFD	Computational Fluid Dynamics
EHL	Elasto-Hydrodynamic Lubrication
FSMI	Fluid-Structure Motion Interaction
LC	Lip Chamber
LP	Lumped-Parameter
RPM	Revolutions Per Minute
VC	Vane Chamber

1 Introduction

Vane pumps are rotary positive displacement machines widely utilized in automotive applications and hydraulic control actuation systems due to their compactness, low noise, and cost efficiency. Among the various design configurations, the balanced twin-lip vane pump is highly suitable for high-pressure applications because its symmetrical porting eliminates net radial loads on the rotor [1]. Furthermore, the twin-lip design allows for pressure compensation mechanisms that handle the critical vane-cam-ring interface, preventing excessive wear [1].

Accurately modeling these units requires capturing the complex interactions of various physical domains. A comprehensive multi-physics baseline simulation model was previously developed by Mistry et al. [1], which coupled fluid dynamics, contact dynamics, lubricating interfaces, and mixed elasto-hydrodynamic lubrication (EHL) into one unified framework. While this baseline model successfully evaluated internal pressures using a lumped-parameter formulation and solved the planar motions of the vanes using Newton's laws of motion, its primary limitation was that the fluid supply flow path through the pump casing was never modeled. Insufficient fluid supply through these unmodeled casing paths can lead to cavitation in the suction port, a phenomenon heavily dependent on fluid properties [2], which could then limit the pump's operational envelope and damage components.

This paper expands upon the previous numerical model [1] to explicitly consider the supply path through the casing. The cartridge unit and the overall fluid flow path are illustrated in Figure 1. Utilizing preliminary CFD simulations, the characteristics of the supply orifices and chambers are defined and integrated into the model. Following geometric analysis, further improvements to the casing channels and the cam-ring orifice are proposed to expand the volumetric efficiency and capacity of the unit at maximum operating speeds (Ω_{max}).

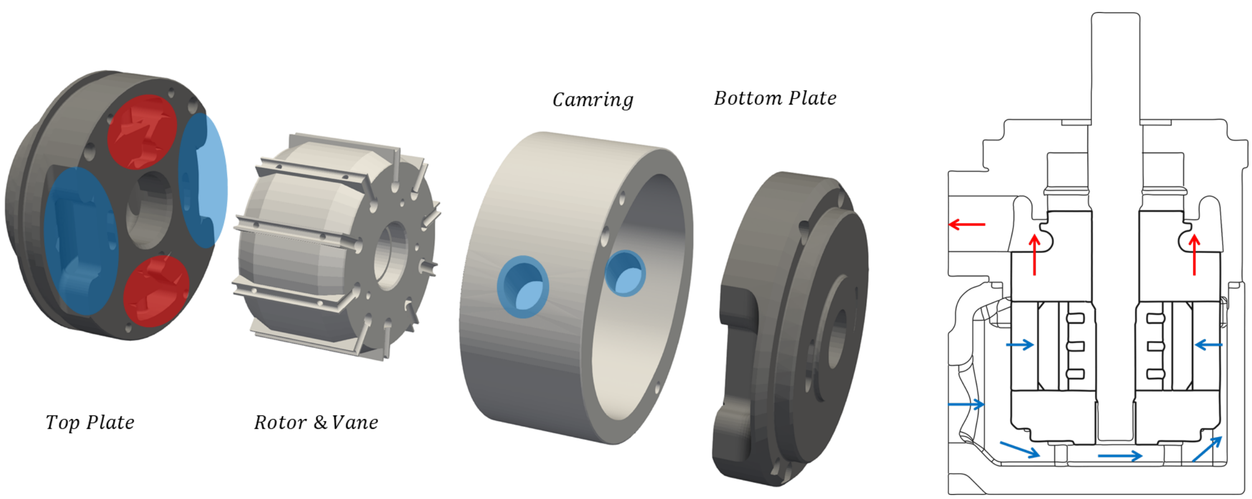

(a) The exploded view of the cartridge unit.

(b) Full unit cross-section view.

Figure 1: *In figure (a), the blue area represents the inlet flow port, and the red area represents the outlet flow port. In figure (b), the outline includes the casing (thinner lines) and the cartridge unit (bold lines), with arrows indicating the flow path and colors corresponding to low and high pressure.*

Several recent studies have focused specifically on the filling capability and cavitation phenomena within vane pumps. Yan et al. [3] utilized 3D Computational Fluid Dynamics (CFD) to capture the cavitation performance of a sliding vane pump; however, their study was restricted to a non-balanced single-lip design and only investigated lower rotational speeds. For balanced vane pumps, Lobsinger et al. [4] performed multi-phase CFD simulations to evaluate the effects of air content on the outlet flow and filling characteristics. Similarly, Stuppioni et al. [5] and Suzuki et al. [6] demonstrated the capability of 3D CFD approaches to model dissolved gas and predict pressure ripples by comparing simulations to measured internal unit pressures. Furthermore, Rundo et al. [7] utilized CFD to analyze how various geometrical features affect the filling behavior of vane pumps operating at high shaft speeds.

While these past works demonstrate that 3D CFD approaches allow for an in-depth analysis of internal flow features—specifically the aeration and vaporization effects intimately related to a unit's filling capability—they possess significant limitations. Because full 3D CFD models are highly computationally expensive, they typically require initial assumptions of fixed gap heights at the critical vane-cam-ring interface. Consequently, they cannot dynamically evaluate the planar motions and tilting of the vanes during operation, which are essential for accurately predicting the torque losses and overall hydromechanical efficiency of the unit.

To overcome these limitations, the methodology proposed in this paper bridges the gap between high-fidelity spatial flow mapping and computationally efficient dynamic modeling. Instead of relying solely on a computationally heavy CFD model or a 1D analytical model, this work utilizes preliminary steady-state CFD simulations to extract the hydraulic restrictions and orifice discharge coefficients of the unmodeled casing paths. These characterized parameters are then directly integrated into a fast, dynamically coupled lumped-parameter framework. This approach successfully captures the high-speed cavitation limitations of the entire unit while preserving the dynamic evaluation of mechanical losses, allowing for rapid geometry optimization that extends the pump's operational speed.

The remainder of this paper is organized as follows. Section 2 introduces the numerical framework, detailing the geometric evaluation and the extended fluid dynamics module. Section 3 describes the CFD characterization used to define the upstream casing parameters. Section 4 presents the simulation results, identifying baseline cavitation limitations. Section 5 introduces the optimized casing geometries with numerical simulation results, and Section 6 outlines the experimental validation. Finally, Section 7 draws the main conclusions of this work.

2 Numerical Framework

The foundation of the numerical framework utilized in this study is a strongly coupled Fluid-Structure Motion Interaction (FSMI) module, which was comprehensively developed, detailed, and experimentally validated in the reference work by Mistry et al. [1]. This baseline architecture is designed to evaluate the highly complex internal physics of a twin-lip balanced vane pump by coupling fluid dynamics, rigid body kinematics, contact mechanics, and mixed Elasto-Hydrodynamic Lubrication (EHL) into a single unified environment. To achieve this, the FSMI framework is structured around fundamental sub-modules operating in tandem, as shown in Figure 2.

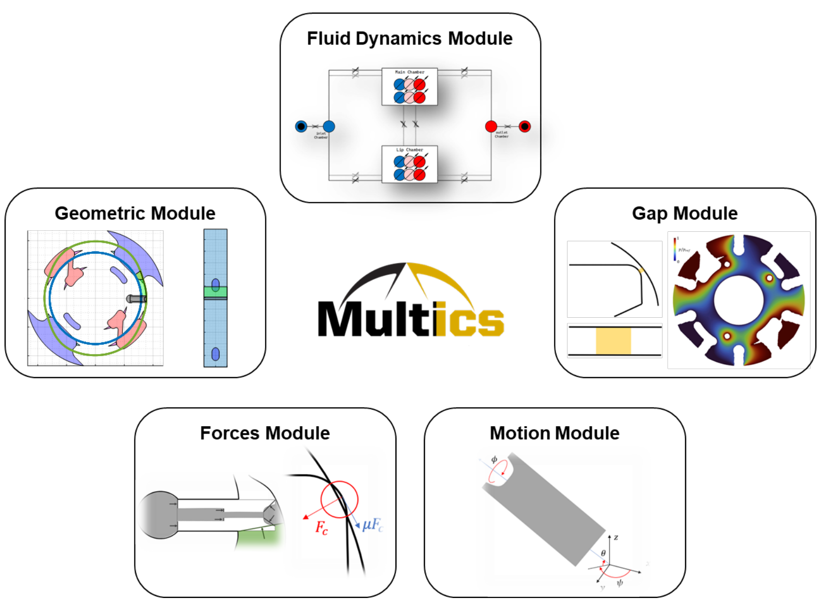

Figure 2: *Overview of the coupled multi-physics simulation architecture.*

This paper focuses on extending the baseline multi-physics model, specifically within the geometric and fluid dynamics aspects, to investigate the cavitation phenomena occurring during high-speed unit operation. While the original framework effectively captured the core cartridge dynamics, it did not account for the upstream casing supply restrictions. The sections below detail the procedural advancements made to capture these effects, highlighting the integration of characterized casing supply pathways and the expansion of the fluid circuit to dynamically track localized density drops and premature cavitation.

2.1 Geometric Model

The geometric module functions as a preprocessor that extracts precise geometrical features based directly on the physical geometry of the pump's internal components. By evaluating this geometry, representative polygons are generated without relying on simplified analytical assumptions [1]. This module calculates the theoretical radial coordinates of the vanes for every degree of shaft rotation by moving the vane profile iteratively until the distance between the vane-lip and cam ring profiles is near zero [1]. By stitching bounding points into closed polygons, the module accurately defines the instantaneous volumes of the two primary fluid control volumes: the Vane Chamber (VC) and the Lip Chamber (LC). Finally, it performs polygon intersections to evaluate the overlapping flow areas between the displacement chambers and the inlet/outlet ports. These geometrical features are stored as a lookup table and supplied to the fluid dynamics module.

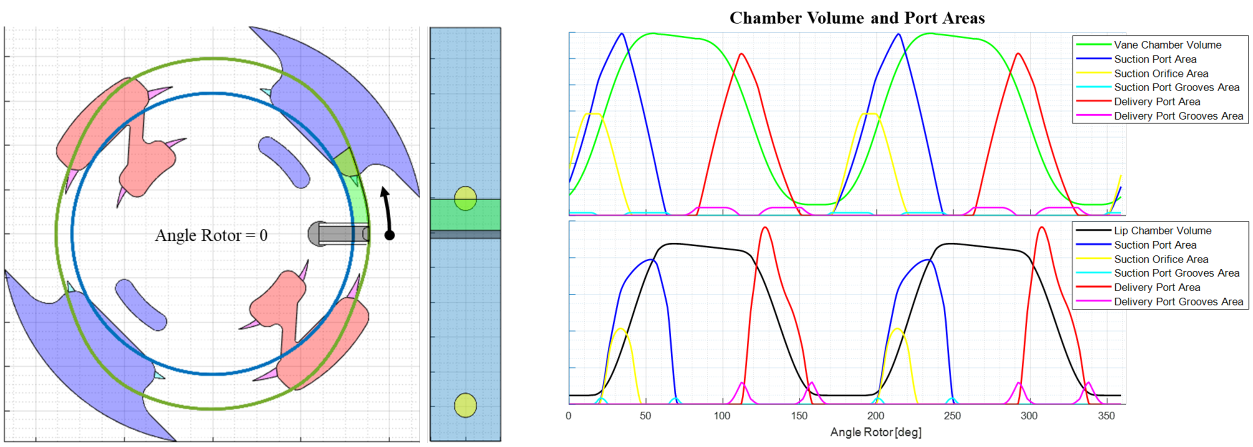

(a) *Lateral plate porting and connections from supply chambers to displacement chambers.*

(b) *Volume and port area variations between displacement and supply chambers.*

Figure 3: *Plot (a) illustrates the geometric shape of the lateral plate port and chamber volume connections at the initial state. Plot (b) illustrates the corresponding areas (y-axis, left) and volumes (y-axis, right) at each angular step (x-axis, from* $0°$ *to* $360°$*).*

The geometry of the Vane Chamber (VC) and Lip Chamber (LC) volumes at different angles is continuously evaluated as the rotor spins. Zero degrees is defined when rotor vane 1 is perfectly horizontal as shown in Figure 3a. At each angular step, the module solves for the instantaneous volume of the displacement chambers and the corresponding connection area between the ports and the chamber volumes. Figure 3b illustrates these chamber volumes and connection port areas at each angular step, which directly dictate the fluid mass transfer in the subsequent fluid dynamics module. To visualize this kinematic progression, Figure 4 demonstrates a displacement chamber undergoing half of a full rotation cycle, and captures the timing of the chamber enters and exits the low-pressure inlet port, as well as its transition into and out of the high-pressure outlet port at various key angular locations.

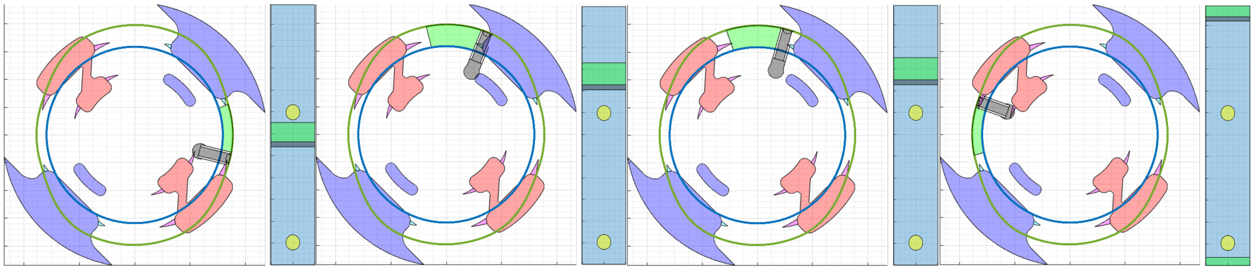

(a) Rotor angle at 346°. *(b) Rotor angle at 68°.* *(c) Rotor angle at 74°.* *(d) Rotor angle at 160°.*

Figure 4: *Demonstration of a displacement chamber undergoing half of a full rotation cycle (blue: inlet port, red: outlet port). The figure illustrates the displacement chamber entering the inlet port at 346° (a), exiting the inlet port at 68° (b), entering the high-pressure outlet port at 74° (c), and exiting the outlet port at 160° (d). Subsequent plots tracking performance across rotor angles directly correspond to these critical port connection points.*

2.2 Fluid Dynamics Module

The fluid dynamics module evaluates the fluid state inside the control volumes using a lumped-parameter approach centered around the fundamental pressure build-up equation [2]. This equation is derived directly from the principle of mass conservation for a variable control volume V_i:

$$\sum \dot{m}_{in,i} - \sum \dot{m}_{out,i} = \frac{d(\rho_i V_i)}{dt} = V_i \frac{d\rho_i}{dt} + \rho_i \frac{dV_i}{dt} \tag{1}$$

To relate the transient changes in localized fluid density (ρ_i) to the internal chamber pressure (p_i), the fluid bulk modulus (K_i) is utilized. Substituting this relationship into Equation 1 yields the pressure build-up equation:

$$\frac{dp_i}{dt} = \frac{K_i}{\rho_i V_i} \left(\sum \dot{m}_{in,i} - \sum \dot{m}_{out,i} - \rho_i \frac{dV_i}{dt} \right) \tag{2}$$

Within this framework, cavitation effects are captured through the pressure-dependent state formulations of density (ρ_i) and bulk modulus (K_i) [1]. The fluid is modeled as a homogeneous mixture of liquid, dissolved air, and free gas/vapor. When the local pressure in the suction chamber drops, the fluid density decreases, and the bulk modulus drops drastically [2]. This dynamic variation signifies the onset of cavitation, allowing the model to accurately track the percentage of gas and vapor bubbles dynamically.

While the baseline model applied this formulation successfully, it previously considered only the core cartridge unit of the pump. Consequently, it assumed an unrestrictive, ideal fluid supply directly to the cartridge inlet ports, neglecting the complex upstream geometries of the pump casing. To accurately capture the high-speed filling limitations of the machine, the fluid dynamic model was extended to explicitly include the complete flow path from the casing inlet to the cartridge inlet. Physically, the hydraulic fluid traverses a tortuous internal pathway, routing from the main inlet chamber to a base chamber via a rectangular-shaped orifice, and continuing from the base chamber through a thin rectangular slot to reach the back chamber of the cartridge.

To maintain high computational efficiency while capturing these spatial restrictions, preliminary steady-state 3D CFD simulations are utilized purely for physical characterization to evaluate the pressure drops across these simplified casing volumes. These extracted parameters are then used to define orifice discharge coefficients (C_d) for each casing segment.

Once characterized, these intricate casing supply pathways are incorporated directly into the LP fluid circuit as upstream variable control volumes connected by variable orifices, as depicted in Figure 5. The fluid dynamics module actively resolves the mass flux through these characterized casing channels, which are situated upstream of the fluid entering the primary VC and LC displacement chambers. By evaluating the pressure restrictions through these upstream casing channels, the extended numerical framework is fully equipped to dynamically track severe fluid density drops and the subsequent onset of cavitation occurring at the cartridge inlet.

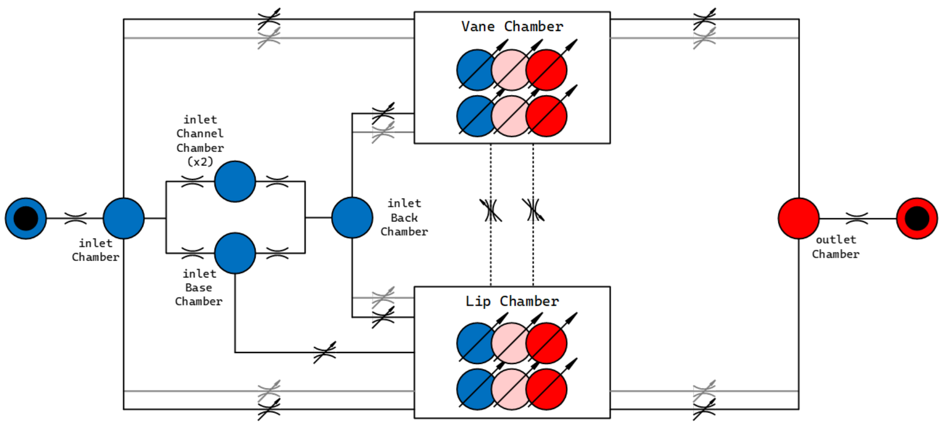

Figure 5: *Lumped-parameter method of the updated fluid path, illustrating how the CFD-characterized casing supply paths are integrated as upstream control volumes into the overall multi-physics framework shown in Figure 2.*

3 CFD Characterization

To accurately capture the hydraulic restrictions prior to the primary suction port, the casing supply path was thoroughly analyzed using CFD. To reduce computational overhead while maintaining strict volumetric fidelity, the 3D CFD model utilized a simplified geometry that preserved the exact fluid volumes and critical cross-sectional areas of the physical pump. Specifically, the modeled fluid domain was discretized into three primary supply pathways. The first pathway routes, in Figure 6, fluid from the inlet chamber to the base chamber via a rectangular-shaped orifice. The second pathway channels fluid from the base chamber through a thin rectangular slot to reach the back chamber. Finally, a third supplementary pathway directs fluid from the inlet through a small channel directly to the back chamber.

The primary objective of these CFD simulations is to characterize the hydraulic resistance of these specific pathways so they can be accurately represented in the 1D lumped-parameter model [1]. This is achieved by determining the orifice discharge coefficient (C_d) for each geometric restriction. The CFD simulations were performed using SOLIDWORKS Flow Simulation software. A steady-state, incompressible pressure-based solver was utilized with a standard $k - \epsilon$ turbulence model to accurately capture the turbulent flow structures. Convergence was monitored by ensuring all residuals dropped below 10^{-4} and mass imbalances were negligible. The simulation methodology prescribes a steady-state nominal mass flow rate ($\dot{m}_{nom}$) under a nominal operating pressure boundary condition. By solving the fundamental Navier-Stokes equations across the simplified spatial domain, the CFD model evaluates the corresponding pressure drop (Δp_{CFD}) that occurs across each volumetric segment.

This methodology leverages the standard orifice loss equation, derived from Bernoulli's principle for flow across a sudden restriction. Considering the fluid as incompressible across the localized restriction, the mass flow rate ($\dot{m}$) is mathematically defined as:

$$\dot{m} = \text{sign}(p_i - p_j) C_d A \sqrt{2\rho |p_i - p_j|} \tag{3}$$

By rearranging this governing equation and substituting the nominal parameters evaluated during the CFD process, the discharge coefficient is explicitly calculated as:

$$C_d = \frac{\dot{m}_{nom}}{A\sqrt{2\rho \Delta p_{CFD}}} \tag{4}$$

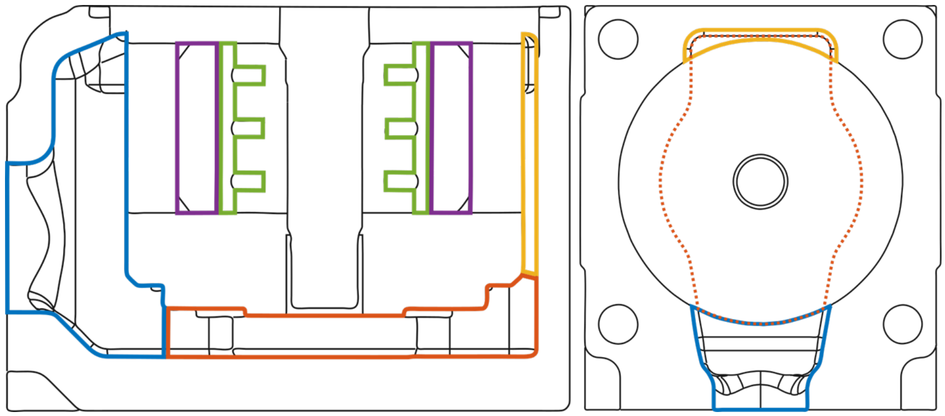

Figure 6: *Each chamber defined in the fluid circuit is highlighted in the pump frame in the left cross-section view; the right figure shows the top view of the lower section flow path with dotted lines indicating routing below the cartridge body.*

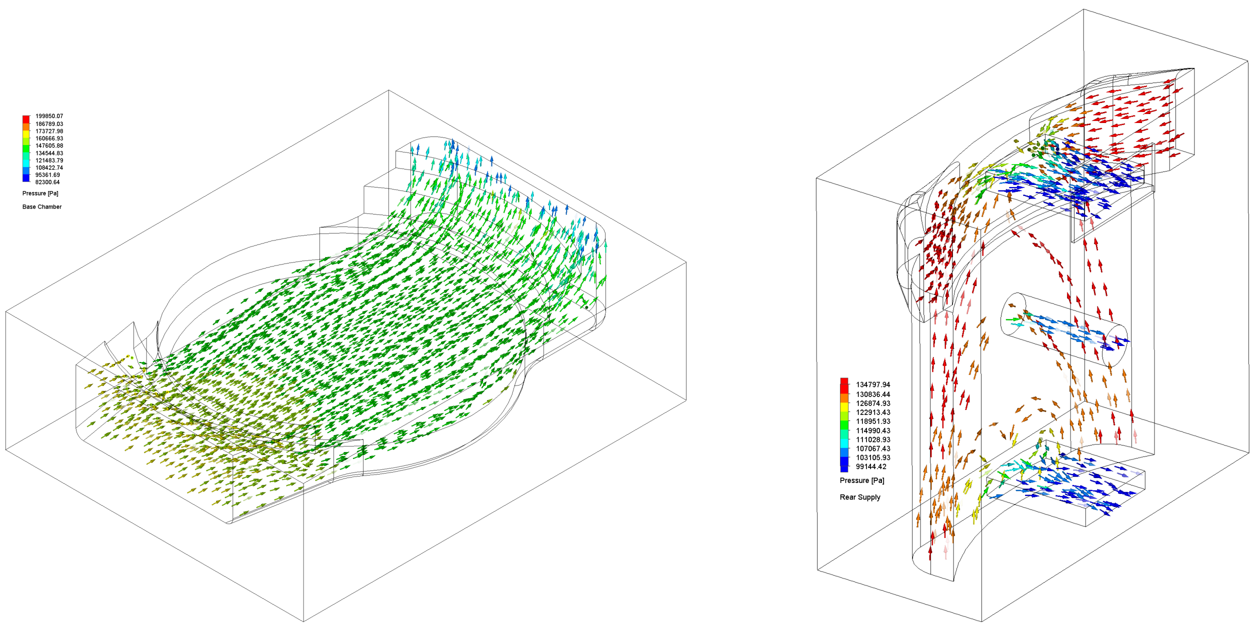

(a) *CFD flow across the inlet base chamber.*

(b) *CFD flow from rear chamber to VC.*

Figure 7: *CFD simulation for each port connection; note the pressure drop (colored) pressure drop across the simplified fluid volumes used to evaluate the discharge coefficients.*

Once these specific discharge coefficients are characterized for their corresponding orifices, they are integrated into the lumped-parameter fluid circuit of the whole unit. As highlighted by the CFD characterization process shown in Figure 7, the characteristic of the orifice varies significantly across the path from the inlet to the cartridge unit. This insight ultimately allowed the numerical model to accurately capture the severe cavitation effect previously observed at the second suction port.

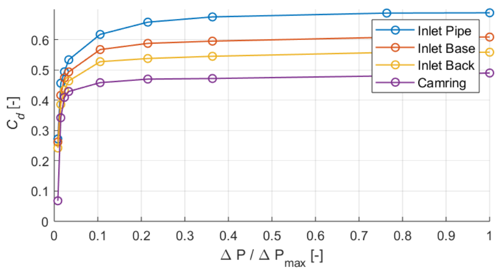

***(a)** Orifice discharge coefficient at different Δp.*

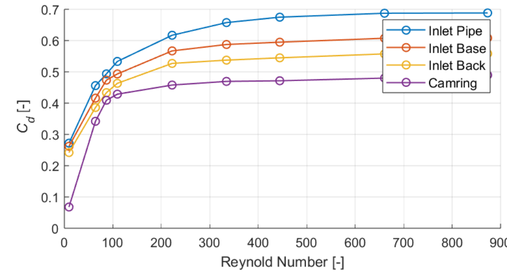

***(b)** Orifice discharge coefficient at corresponding Reynolds number.*

***Figure 8:** CFD simulation results evaluating the discharge coefficients (a) and critical Reynolds transition points (b) for each geometric restriction.*

Figure 8 presents the results from the CFD characterization, highlighting the distinct discharge coefficients (C_d) and critical Reynolds numbers (Re_{crit}) for the different port connections. The precise evaluation of C_d is of paramount importance, as it actively dictates the magnitude of the pressure drop across each specific geometric restriction for a given mass flow rate, effectively capturing the localized flow contraction (vena contracta) and viscous losses. Furthermore, identifying the critical Reynolds number (Re_{crit}) is essential for the lumped-parameter fluid circuit. Re_{crit} defines the specific flow condition at which the fluid transitions from a laminar regime to a turbulent regime. Capturing this transition point allows the 1D model to accurately switch between linear and quadratic flow-pressure relations, ensuring a high-fidelity evaluation of the hydraulic resistance across all operating speeds.

4 Simulation Results

Prior to evaluating the performance improvements of the newly proposed casing and cam ring designs, it is crucial to establish the baseline parameters and fundamental assumptions of the multi-physics simulation. The model evaluates a reference balanced twin-lip vane pump operating with an ISO VG 46 mineral hydraulic fluid. The operating conditions and outcomes are normalized relative to the unit's selected operating speed (Ω_{max}) to protect proprietary data, while the nominal operating temperature is fixed at 25°C. The primary fluid properties, structural material constants, and surface features utilized in the simulation are defined in Table 2.

***Table 1:** Pump specifications.*

Manufacturer	Veljan Denison Limited
Model Number	VT6C025
Displacement	79.3 cm^3/rev
Maximum Pressure	280 bar
Maximum Speed	2800 rev/min
Number of Vanes	10

Several key assumptions are made to maintain computational efficiency while preserving physical fidelity throughout the simulation. First, the fluid dynamics module assumes isothermal flow conditions within the control volumes. Second, while the pressure plates undergo significant deformation under high-pressure loads, structural analysis indicates that the inward deformation of the over-compensated bottom plate and the outward deformation of the top plate effectively reduce the net load to have constant gap height. Additionally, the dynamic contact and friction forces at the critical vane-cam-ring interface are evaluated using a mixed Elasto-Hydrodynamic Lubrication (EHL) formulation [1], which is a well-proven physical phenomenon dictating these interactions. This formulation relies directly on the measured surface roughness and radius of curvature of the contacting steel components.

Table 2: *Simulation Parameters*

Fluid Properties	
Temperature (T)	40 °C
Atmospheric Pressure (p_{atm})	1.01325×10^5 Pa
Dissolved Air Volume Fraction (α_{air})	0.08 -
Atmospheric Density (ρ_{atm})	860 kg/m^3
Atmospheric Kinematic Viscosity (ν_{atm})	46×10^{-6} m^2/s
Structural & Material Properties	
Young's Modulus (E)	287×10^9 Pa
Coefficient of Restitution (c_e)	0.78 -
Surface Roughness	0.2 μm
Radius of Curvature	Undisclosed

4.1 Flow Behavior

Before evaluating the newly proposed optimized geometries, the extended whole-unit fluid dynamic model was tested to ensure it maintained the accuracy established by the baseline cartridge-only model, which has been experimentally validated in the past. The simulation of the updated fluid circuit was run across standard operational ranges and validated against existing experimental results.

As illustrated in Figure 9(a), the integration of the casing supply pathways demonstrates excellent agreement with the original cartridge-only model [1]. Specifically, the modified simulation accurately matches the original model predictions for volumetric efficiency prior to the onset of severe cavitation limitations. Furthermore, Figure 9(b) illustrates the baseline pressurization of the Vane Chamber (VC) and Lip Chamber (LC) in one complete cycle, behaving as expected. The model perfectly captures the inherent transient delivery features and outlet flow behavior, aligning with the periodic shape and amplitude of the experimentally measured pressure ripples. This baseline alignment confirms that integrating the upstream casing restrictions via characterized orifice coefficients does not disrupt the fundamental physics of the internal displacement cycle. While the original model assumed ideal filling and thus overpredicted volumetric efficiency at high speeds, the current extended model successfully captures the efficiency drop-off due to casing restrictions, aligning more closely with the observed physical limits, as detailed in the following sections.

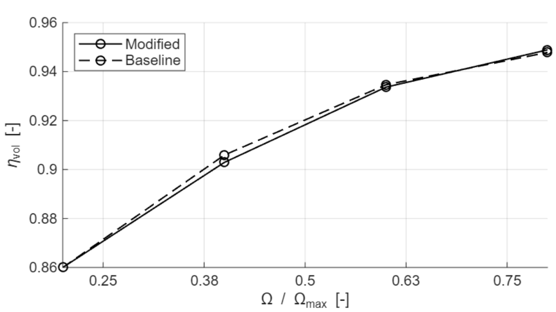

(a) *Model efficiency comparison.*

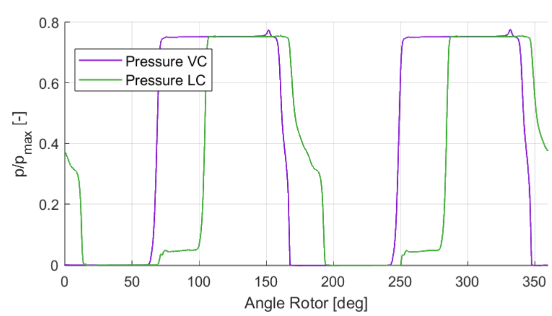

(b) *Displacement chambers pressure in one cycle.*

Figure 9: *Left figure shows that the modified simulation model matches the original baseline model predictions. Right figure shows the displacement chamber VC and LC pressurization for one cycle.*

4.2 Chamber Cavitation

While the baseline model successfully predicted performance at standard speeds, it was designed to capture the cartridge unit performance without considering the supply path in the casing. By updating the fluid circuit to consider the true geometry of the casing flow paths, the extended simulation successfully captures the severe fluid density drops and pressure restrictions occurring prior to the main displacement chambers.

Leakage at the vane tip in contact with the cam-ring varies as the chamber enters and exits the high-pressure region. Increasing the operating RPM alters the pressure distribution in the EHL contact, varying the gap height. These discrepancies closely correlate with the inter-chamber leakages that dictate the unit's final volumetric efficiency.

As the rotational speed of the pump increases, the displacement chambers demand a significantly higher mass flow rate during the suction phase. In the physical unit, fluid entering the primary casing inlet must navigate a tortuous path to reach the rear of the cartridge, traversing from the inlet chamber to the base chamber, and finally squeezing through a thin rectangular slot to reach the back chamber. The lumped-parameter model dynamically calculates the pressure drop across these geometric bottlenecks. At elevated speeds, this severe hydraulic restriction causes the localized pressure within the casing channels to plummet.

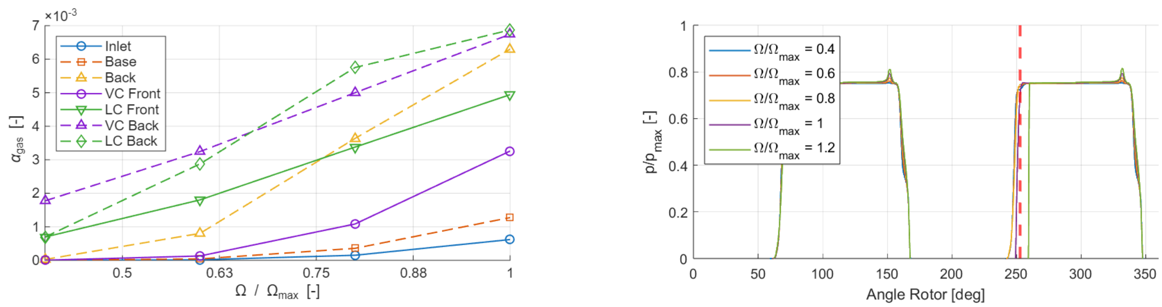

(a) *Gas fraction in each chamber.*

(b) *Displacement chamber pressure in one cycle.*

Figure 10: *Lumped-parameter simulation of the internal casing path illustrating that the chambers are cavitating (a), and the delayed pressurization (b) confirming this event.*

The simulation reveals a critical phenomenon, visualized in Figure 10(a): as the pressure drops below the fluid's saturation and vapor pressures, the localized fluid density and bulk modulus decrease drastically. This triggers premature aeration and vaporization within the casing itself—effectively a "pre-cavitation" event occurring well before the fluid even crosses the suction port boundary into the Vane Chamber (VC) and Lip Chamber (LC). Figure 10(a) presents the simulation results showing the percentage of free gas and vapor across the different chambers. The back displacement chamber and its corresponding upstream supply chambers indicate significant cavitation occurring at much earlier phases of operation compared to the adequately supplied front chambers.

By explicitly tracking these localized fluid properties throughout the entire unit, the model directly links the upstream casing restrictions to the onset of severe suction port cavitation. The simulation demonstrates that the displacing chambers are unevenly filled. Because the fluid must travel through the highly restrictive thin port to reach the back chamber, the second suction port experiences high cavitation effect.

This physical limitation is further illustrated by evaluating the pressure within the displacement chambers at various normalized operating speeds (Ω/Ω_{max}). As seen in Figure 10(b), the VC experiences a significantly delayed pressurization when operating at higher rotational speeds. This delay at the second inlet is a direct consequence of the upstream pre-cavitation choking the supply flow, coupled with the chamber's own localized cavitation. As the pump operating RPM increases, the restrictive upstream casing pathways choke the flow, forcing the displacement chambers drawing from this rear port to ingest a vapor-heavy mixture, leaving them severely under-filled compared to the front chambers.

5 Geometry Modification

To mitigate the cavitation effects identified in the baseline unit, an updated geometry was proposed and analyzed. The geometries were iteratively modified to expand the cross-sectional areas within the allowable manufacturing constraints, rather than using a formal optimization algorithm. The original restrictive casing channels were primarily a result of conservative manufacturing tolerances and spatial constraints within the pump housing. Expanding these channels does not compromise the structural integrity of the casing, provided the minimum wall thickness requirements are maintained.

The fundamental mechanism driving the pre-cavitation is the excessive localized pressure drop caused by flow constriction. Based on the preliminary CFD investigations, the primary casing modifications included geometrically expanding the internal casing channels—specifically increasing their respective radii and widening the gap between the cartridge and the casing wall. These physical modifications effectively increase the cross-sectional area of the supply pathways.

According to the principles of fluid dynamics, expanding the cross-sectional area proportionally reduces the localized fluid velocity. Consequently, the dynamic pressure losses are minimized, allowing the absolute pressure within the casing channels to remain above the fluid's saturation and vapor pressures. By characterizing these newly expanded geometries with CFD, updated orifice discharge coefficients (C_d) were derived and integrated into the lumped-parameter fluid circuit. The significance of these updated characteristics is most accurately captured by the model's ability to simulate cavitation dynamically.

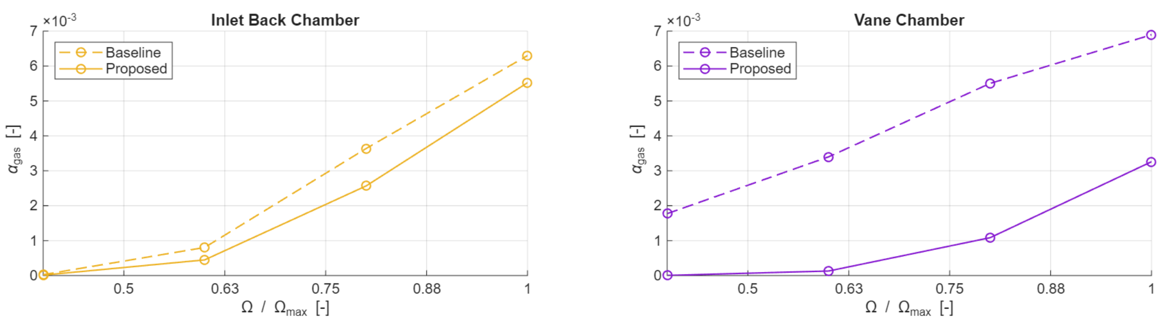

(a) *Gas fraction in the inlet back chamber.* ***(b)*** *Gas fraction in the vane chamber.*

Figure 11: *Simulation results comparing the gas fraction in the displacement chambers, demonstrating significantly reduced aeration and cavitation with the optimized casing design.*

As shown in Figure 11, simulating the expanded geometry with the new orifice characteristics demonstrates a drastic reduction in the free gas percentage within the back chamber compared to the baseline model. By minimizing the upstream restriction, the fluid flow reaching the second suction port maintains a density equivalent to that of the front chamber, successfully mitigating the severe pre-cavitation effects.

These geometric modifications successfully suppress the premature release of dissolved air and the vaporization of the hydraulic fluid. Consequently, the simulation predicts a significant increase in volumetric efficiency at elevated operational speeds. In the baseline experimental data, the pump's operation was strictly limited, with distinct signs of efficiency decreases beginning at mid-range speeds due to incomplete filling. However, with the newly proposed casing design, the simulation indicates that the updated design will allow the unit to reduce cavitation, enabling operation at higher speeds. These numerical predictions are scheduled for experimental validation.

6 Experimental Validation

6.1 Test Rig Setup

To validate the simulation predictions and quantify the performance improvements of the optimized fluid supply paths, an experimental test rig built at the authors' research lab was utilized. The hydraulic circuit is designed to precisely control the operating conditions and measure the steady-state performance of the prototype. The layout of the test rig is illustrated in Figure 12. A needle valve was used as a loading element to set the desired pressure at each operating shaft speed. Additionally, a sharp edge fixed orifice and a calibrated pipe (with a constant diameter of 16 mm and length of 200 mm) were placed at the pump outlet; this setup allowed for the establishment of standing waves for pressure ripple tests. The prime mover drives the pump while absolute pressure sensors monitor the inlet and outlet pressures, which is critical for identifying the onset of cavitation vacuum. A flow meter measures the delivery flow rate, and temperature sensors track the thermal state of the fluid. Prior to testing, an optical profilometer (Bruker NPFLEX-1000) was used to measure the critical surface features of the components, such as the roughness and radius of curvature of the vane-lips. The details and accuracies of the sensors used are listed in Table 3.

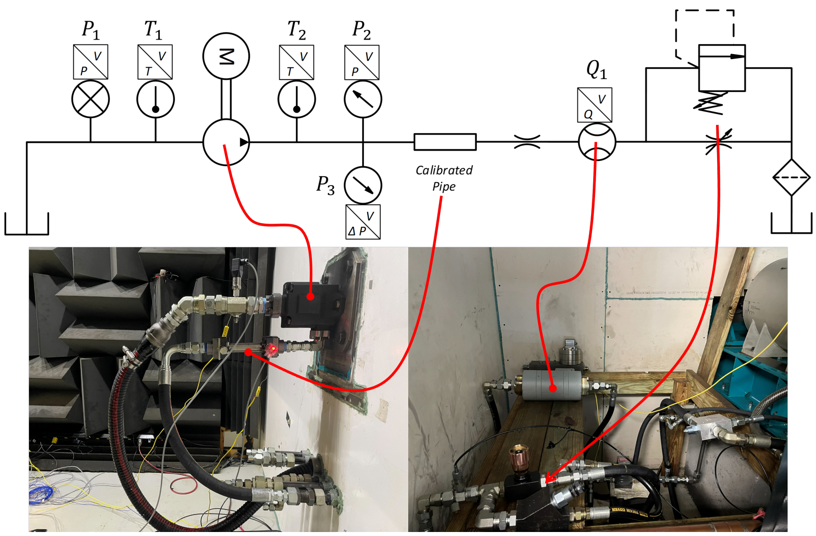

Figure 12: *Schematic drawing of the experimental test rig used to evaluate the pump's performance and photograph of the physical experimental test rig installation.*

Table 3: *Sensor specifications.*

Sensor	Type	Description
T_1, T_2	Thermocouple	OMEGA, scale: 0 °C to 200 °C, 0.4% FS accuracy
P_1	Strain gauge	WIKA, scale: 0–1.6 barA, 0.125% FS accuracy
P_2	Piezoelectric (quartz)	KISTLER, scale: -1–10 bar, 13 kHz natural frequency, 0.8% FS accuracy
P_3	Piezoresistive	WIKA, scale: 0–345 bar, 0.5% FS accuracy
Q_1	Gear Flow meter	VSE RS400, scale 1–400 l/min, 0.25% measured value accuracy

6.2 Results

The steady-state flow performance of the newly proposed geometry was experimentally evaluated across its operational envelope and directly compared against the physical baseline design.

As illustrated in Figure 13a, the flow rate of the optimized design scales proportionally with the shaft speed, demonstrating improved delivery characteristics at higher operating conditions compared to the baseline unit. When evaluated in terms of volumetric efficiency (Figure 13b), the experimental validation indicates that the proposed design maintains higher performance levels across the elevated speed range. Whereas the baseline unit experienced a reduction in efficiency attributed to incomplete chamber filling, the optimized casing flow paths effectively mitigate this suction restriction. Consequently, the modified design sustains high volumetric efficiency up to the maximum operating speed, verifying the success of the geometric improvements.

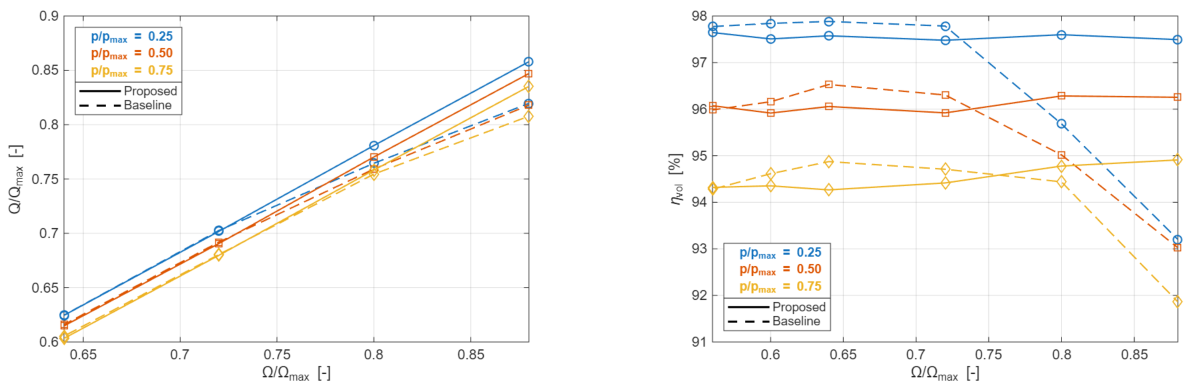

(a) Flow Rate

(b) Volumetric Efficiency

Figure 13: *Experimental validation comparing the steady-state flow rate (a) and volumetric efficiency (b) between the baseline and optimized pump designs.*

7 Conclusion

This paper details the further development of a multi-physics numerical model for balanced twin-lip vane pumps to include the previously unmodeled casing fluid supply paths. Preliminary CFD simulations were used to define the characteristics of the orifices and chambers, allowing the model to capture destructive cavitation effects in the casing. The baseline numerical model was successfully validated against existing experimental results to confirm its fidelity. Subsequently, geometry updates were proposed and characterized via CFD, resulting in a newly designed parameter set that demonstrates improved supply flow capability. By physically expanding the casing channels and further updating the cam-ring orifice, flow velocities and dynamic pressure drops were minimized. Simulation results predict drastically improved performance of the pump at high speeds, resolving the premature cavitation limitations observed in the baseline unit. These numerical predictions and geometric modifications are confirmed through experimental validation, which proves the optimized design's ability to maintain high volumetric efficiency and linear flow delivery at elevated operational speeds.

References

[1] Z. Mistry, A. Vacca, S. K. Uppaluri, “Modeling and experimental validation of twin lip balanced vane pump considering micromotions, contact mechanics, and lubricating interfaces,” *Simulation Modelling Practice and Theory*, vol. 133, p. 102914, 2024.

[2] A. Vacca, G. Franzoni, *Hydraulic Fluid Power*, Wiley, 2021.

[3] Z. Yan, et al., “Structural design and cavitation performance research of single-acting sliding vane pump under high rotational speed and petroleum medium,” *Proc. IMechE Part C: J. Mechanical Engineering Science* (Sage Journals), vol. 239, no. 1, 2023.

[4] T. Lobsinger, T. Hieronymus, and G. Brenner, “A CFD investigation of a 2D balanced vane pump focusing on leakage flows and multiphase flow characteristics,” *Energies*, vol. 13, no. 13, 2020.

[5] U. Stuppioni, A. Suman, M. Pinelli, and A. Blum, “Computational fluid dynamics modeling of gaseous cavitation in lubricating vane pumps: An approach based on dimensional analysis,” *Journal of Fluids Engineering*, vol. 142, no. 7, p. 071206, 2020.

[6] K. Suzuki, Y. Nakamura, S. Yakabe, H. Watanabe, and K. Nakamura, “Characteristics prediction of vane pump by CFD analysis,” *KYB Technical Review*, vol. 53, pp. 8–15, 2016.

[7] M. Rundo, G. Altare, and P. Casoli, “Simulation of the filling capability in vane pumps,” *Energies*, vol. 12, no. 2, 2019.